Feedback-induced oscillations in one-dimensional colloidal transport

K. Lichtner,[1,*] A. Pototsky,[2] and S. H. L. Klapp[1]

[1]*Institute of Theoretical Physics, Secr. EW 7-1, Technical University Berlin, Hardenbergstr. 36, D-10623 Berlin, Germany*
[2]*Department of Mathematics, University of Cape Town, Rondebosch 7701, South Africa*

We investigate a driven, one-dimensional system of colloidal particles in a periodically corrugated narrow channel subject to a time-delayed feedback control. Our goal is to identify conditions under which the control induces oscillatory, time-periodic states. The investigations are based on the Fokker-Planck equation involving the density distribution of the system. First, by using the numerical continuation technique, we determine the linear stability of a stationary density. Second, the nonlinear regimes are analyzed by studying numerically the temporal evolution of the first moment of the density distribution. In this way we construct a bifurcation diagram revealing the nature of the instability. Apart from the case of a system with periodic boundary conditions, we also consider a microchannel of finite length. Finally, we study the influence of (repulsive) particle interactions based on dynamical density functional theory.

I. INTRODUCTION

The study of transport of particles in complex geometries is a major topic in nonequilibrium statistical physics with relevance in diverse fields such as biology, condensed matter, and nanotechnology [1,2]. Exemplary systems are colloids in optical (or otherwise modulated) potentials [3–6], (bio-)molecules in microchannels [7], cold atoms in optical lattices [8], and magnetic particles adsorbed on ferrimagnetic garnet films [9]. Depending on the details of the (often one-dimensional) potential, a variety of fascinating effects can been observed, including ratchet mechanisms [10], giant diffusion [11], and anomalous (subdiffusive) transport [12–15]. For colloids, which are typically of the size of nano- to micrometers, many of these effects can be monitored by real-space experiments (see, e.g., Refs. [16–19]).

In the present paper we investigate a one-dimensional colloidal system where the force exerted by the (static) modulated potential is supplemented by a *feedback control* force, i.e., a force depending on the state of the system. Feedback control in the context of Brownian systems is a focus of growing interest, and the method has already been applied, on a theoretical level, to Brownian motors [20,21] and flashing or rocking ratchets [22]. Moreover, a first experimental realization of a feedback-controlled flashing ratchet already exists [23]. The overall goal of the feedback control in this context is to manipulate and/or optimize transport properties such as the current in a flashing ratchet. Beyond this more applicational motivation, feedback-controlled transport phenomena are also of fundamental interest due to the subtle interplay between state-dependent control protocols, thermodynamics, and information theory [24,25]. Very recently, a colloidal system under feedback control was used as experimental realization of an "information heat engine" [26].

Following an earlier study by two of us [27], we here employ a feedback control with delay where the control term involves the difference between an system variable (the control target) at time t and its value at time $t − \tau$, with τ being the delay time. Such a time delay often occurs in experiments due to the time lag between measurement and feedback. In the general context of control of nonlinear system [28], time-delayed feedback control (which was introduced by Pyragas [29]) has been proven to be extremely efficient, e.g., for the stabilization of chaotic orbits; however, steady states can be manipulated as well. In [27] we used the delayed feedback control to manipulate the current of interacting colloids driven through in a tilted washboard potential. Indeed, it turned out that the control can optimize the current and even yield a current reversal, similar to what has been previously seen for noninteracting systems [30,31].

In the present study we go one step further and ask to what extent the time-delayed feedback control can induce dynamic states *not seen* in the uncontrolled system, which involves a purely static potential. Specifically, we search for the existence of spatiotemporal structures characterized by an *oscillatory* distribution of particles. That time-delayed feedback control itself can indeed generate novel dynamics has recently also been seen in other extended systems [32]. More specifically, we show that the existence and stability of the oscillatory distribution density strongly depends on the properties of the periodic energy landscape that describes the interaction between the particle and the channel walls. The energy landscape, in its turn, is directly linked to the properties of the individual particles, such as, for instance, the (gyration) radius of the particles. As a consequence, the proposed time-delayed feedback control can be used as a filter in order to separate particles of different size. The underlying mechanism is somewhat similar to the well-studied symmetry-selected sorting of particles in periodic potential landscapes [33,34].

Our investigations are based on the numerical solution of the nonlinear Fokker-Planck equation combined with a linear stability analysis. Thus, the basic dynamic variable is the time-dependent density field. Similarly to our previous study [27] our control protocol involves the average particle position as a control target, a quantity which is, in principle, accessible by experiments. We investigate both infinite systems, that is, colloidal particles on a ring (see Ref. [16] for an experiment), and a finite system to which we refer as microchannel geometry

───────
*lichtner@mailbox.tu-berlin.de

[35]. For both geometries, we do indeed find oscillatory states at appropriate system parameters and finite values of the control strength and the delay time. The character of these oscillations, on the other hand, strongly depends on the setup.

In the last part of the paper, we briefly discuss the impact of repulsive interactions between the particles. This is done on the basis of dynamical density functional theory (DDFT), where the microscopic interactions enter via the free energy functional. Indeed, in the past several years DDFT has been applied to a variety of driven colloidal systems [36], including attracting colloidal particles in 1D (time-dependent) ratchet potentials [37].

The rest of the paper is organized as follows. Section II contains the formulation of the problem. In Sec. III, we determine the stability of a nontrivial stationary, spatiallyperiodic density distribution by linearizing the Fokker-Planck equation subject to a time-delayed control force. For the nonlinear regimes, we provide numerical solutions of the (full) Fokker-Planck equation and construct a bifurcation diagram based on monitoring the amplitude of the solutions. In Sec. IV, we discuss the impact of the channel geometry on the oscillation instability. For that purpose, we consider a microchannel of finite length L and follow the same procedure as for the infinite system. The role of interactions between the particles is briefly discussed in Sec. V.

II. THEORY

Our model system consists of overdamped colloidal particles in a one-dimensional channel of length L. The particles are subject to a spatially periodic, symmetric "washboard" potential $U_{\text{wb}}(z) = U_0 \cos^2(kz)$, where k defines the wavelength and U_0 is the amplitude. Henceforth, we set $k\sigma = 1$, where σ corresponds to the effective radius of the particle. For a colloidal particle with spherical symmetry, σ is just the radius of the sphere while, for a polymer, σ is the radius of gyration. The washboard potential is tilted by a constant force $\mathbf{F}_{\text{bias}} = F_0 \hat{\mathbf{z}}$ (with $\hat{\mathbf{z}}$ being the unit vector in the z direction) corresponding to a linear potential $U_{\text{bias}} = -F_0 z$. The tilting leads to an effective motion of the particles in the direction of $\text{sign}(F_0)$ along the z axis. In addition to these static potentials, we assume that the particles are subject to a time-delayed feedback control force of the form [27]

$$F_{\text{fb}}(t,\tau) = -K_0\{1 - \tanh[\bar{f}(t) - \bar{f}(t-\tau)]\}, \quad (1)$$

where $\bar{f}(t)$ is a space-averaged coupling function which depends on the internal dynamical variables of the system. Specifically, we set

$$\bar{f}(t) = \int_{z_0}^{L+z_0} f(z)\rho(z,t)\,dz, \quad (2)$$

with z_0 being the coordinate of the origin of the z axis. Note that when the feedback term is switched on, the effective constant driving force is given by $\gamma = F_0 - K_0$.

In Ref. [27], we used a force of type (1) to manipulate or, more precisely, to revert the net current induced by the biasing force. Here, we aim to explore to which extent such a feedback force can induce oscillatory (time-periodic) density states, which correspond to synchronized oscillations of the particles along the channel. We note that the control force

in Eq. (1) is of Pyragas type [29], i.e., the difference of the "control target" at time t and its value at time $t - \tau$ is used as input for the feedback loop, where τ is called "delay time" and K_0 is the control amplitude. We stress that the ansatz for the feedback force in Eq. (1) is clearly of heuristic nature and thus cannot be derived from any physical potential.

Collecting all external contributions gives the total external potential

$$\begin{aligned}
U_{\text{ext}} &= U_{\text{wb}}(z) + U_{\text{fb}}(t,\tau) + U_{\text{bias}}(z) \\
&= U_0 \cos^2(z) + K_0 z(1 - \tanh[\bar{f}(t) - \bar{f}(t-\tau)]) - F_0 z,
\end{aligned} \quad (3)$$

where we assumed that the contribution of the feedback force is linear in the position coordinate z. In the absence of interactions between the particles, their Brownian motion is governed by the following Fokker-Planck equation [38]:

$$\Gamma^{-1}\frac{\partial \rho(z,t)}{\partial t} = k_B T \frac{\partial^2 \rho(z,t)}{\partial z^2} - \frac{\partial}{\partial z}[\rho(z,t)\tilde{\mu}(z,t;\tau)], \quad (4)$$

where the drift coefficient $\tilde{\mu}$ can be calculated from the external potential U_{ext} via $\tilde{\mu} = -U'_{\text{ext}}$, where $'$ denotes the derivative with respect to z. The mobility coefficient in Eq. (4) is related to the diffusion constant via $\Gamma = \beta D_0$ [where $\beta = 1/(k_B T)$] and we set its value to $\Gamma \tau_B k_B T/\sigma^2 = 1$. Time is measured in units of the Brownian time scale $\tau_B = \sigma^2/(\Gamma k_B T)$, which is of the order of 10^{-9} s for typical Brownian particles.

In the following, we choose a positive value for F_0 such that the particles move preferentially to the right when the control force is being switched off. Also, for the main part of our investigations, we consider the system to be infinitely extended ("circular ring"), that is, we apply periodic boundary conditions over a length L, which is a multiple of a period of the washboard potential, i.e., $L = n\pi\sigma$, with $n = 1,2,\ldots$. However, in Sec. IV, we also discuss the effect of finite channel length.

III. DELAY-INDUCED INSTABILITY

In the absence of control ($K_0 = 0$), the driven system ($F_0 > 0$) settles into a stationary, nonoscillatory state. The corresponding distribution $\rho_s(z)$ can be found analytically [10]

$$\begin{aligned}
\rho_s(z) &= e^{-U_{\text{ext}}(z)/k_B T} \int_z^{L+z} dy\, e^{U_{\text{ext}}(y)/k_B T}/\mathcal{N}, \\
\mathcal{N} &:= \int_{z_0}^{L+z_0} dz \int_z^{L+z} dy\, e^{U_{\text{ext}}(y) - U_{\text{ext}}(z)/k_B T},
\end{aligned} \quad (5)$$

where U_{ext} is the external potential given in Eq. (3) but with $K_0 = 0$ [or, equivalently, $\bar{f}(t) - \bar{f}(t-\tau) = 0$ since we assumed stationarity].

In the presence of control, the behavior of the system depends on the interplay of the parameters of the control term, on the one hand, and the tilted washboard potential, on the other hand. For certain parameter combinations, we still find a stationary state, in which the difference $\bar{f}(t) - \bar{f}(t-\tau)$ disappears. However, as we will demonstrate, for suitable parameters the stationary distribution may become unstable, leading to a stable time-periodic distribution $\rho(z,t)$. To interpret this instability, it is useful to reconsider Eqs. (1) and (2) from a somewhat different perspective. In particular,

since the control target $\bar{f}(t)$ involves a spatial integral over the entire distribution $\rho(z,t)$, we have effectively introduced a coupling between the colloidal particles. Moreover, this coupling is of infinite range (within the periodic system considered). Thus, the time-delayed feedback control introduces an effective interaction of mean-field type, and it is this interaction which may lead to new stationary states, as well as new dynamic regimes, associated with time-periodic density oscillations. We note that the particular type of feedback used here is of purely heuristic nature. This implies that the Fokker-Planck equation Eq. (4) cannot be directly translated into a corresponding system of coupled Langevin equations.

A. Linear stability analysis

We start by applying a linear stability analysis in order to investigate the impact of the delayed feedback control. To this end, we rewrite the dimensionless Fokker-Planck equation in terms of the effective potential $U_{\mathrm{eff}} = U_0 \cos^2 z + (K_0 - F_0)z$ as follows:

$$\frac{\partial \rho(z,t)}{\partial t} = \frac{\partial^2 \rho(z,t)}{\partial z^2} + \frac{\partial}{\partial z}\left[\rho(z,t)\frac{\partial U_{\mathrm{eff}}}{\partial z}\right]$$
$$- K_0 \tanh[\bar{f}(t) - \bar{f}(t-\tau)]\frac{\partial \rho(z,t)}{\partial z}. \quad (6)$$

The nontrivial stationary state $\rho_s(z)$ satisfies

$$0 = \frac{\partial}{\partial z}\left[\rho_s \frac{\partial U_{\mathrm{eff}}}{\partial z} + \frac{\partial \rho_s(z)}{\partial z}\right], \quad (7)$$

which can be written as an eigenvalue problem,

$$\hat{L}\rho_s = \lambda \rho_s, \quad (8)$$

with the stationary Fokker-Planck operator $\hat{L} = \partial_z^2 + (\partial_z U_{\mathrm{eff}})\partial_z + \partial_z^2 U_{\mathrm{eff}}$ and zero eigenvalue $\lambda = 0$.

We are interested in the onset of an oscillatory instability of ρ_s. Following the approach developed earlier [39,40], we set

$$\rho(z,t) = \rho_s(z) + \epsilon[C(z)\cos\omega t + S(z)\sin\omega t], \quad (9)$$

where ϵ is the (small) amplitude of the perturbation, ω is the unknown onset frequency, and the unknown functions $C(z)$ and $S(z)$ determine the shape of the perturbation. With this ansatz, Eq. (6) can be linearized in ϵ to yield

$$-\omega C \sin\omega t + \omega S \cos\omega t = C'' \cos\omega t + S'' \sin\omega t$$
$$+ \partial_z[U_{\mathrm{eff}}'(C\cos\omega t + S\sin\omega t)]$$
$$- K_0 \rho_s'[\bar{f}(t) - \bar{f}(t-\tau)], \quad (10)$$

where $'$ stands for the derivative with respect to z and the perturbed mean field is given by

$$\bar{f}(t) = \langle C \rangle \cos\omega t + \langle S \rangle \sin\omega t, \quad (11)$$

with $\langle C \rangle = \int_{z_0}^{L+z_0} f(z)C(z)\,dz$ and $\langle S \rangle = \int_{z_0}^{L+z_0} f(z)S(z)\,dz$. The initial moment of time can always be chosen in such a way that, for instance, $\bar{f}(t) = \cos\omega t$. This implies two additional integral conditions on the functions $C(z)$ and $S(z)$

$$\int_{z_0}^{L+z_0} f(z)C(z)\,dz = 1, \quad \int_{z_0}^{L+z_0} f(z)S(z)\,dz = 0. \quad (12)$$

The difference $\bar{f}(t) - \bar{f}(t-\tau)$ then becomes

$$\bar{f}(t) - \bar{f}(t-\tau) = \cos\omega t(1 - \cos\omega\tau) - \sin\omega t \sin\omega\tau. \quad (13)$$

Finally, equating the coefficients of $\sin\omega t$ and $\cos\omega t$ in Eq. (10), we obtain two coupled equations for the unknown functions $C(z)$ and $S(z)$,

$$S'' = -\omega C - \partial_z[U_{\mathrm{eff}}S] - K_0 \sin\omega\tau \rho_s',$$
$$C'' = \omega S - \partial_z[U_{\mathrm{eff}}C] + K_0(1 - \cos\omega\tau)\rho_s'. \quad (14)$$

In order to find the stability threshold, one needs to solve Eqs. (14) simultaneously with Eq. (8). To this end, we proceed as follows. We rewrite Eqs. (8) and (14) as an autonomous dynamical system of seven first-order equations, including the equation for z, which takes the form $z' = 1$. The total number of the system parameters is thereby extended by two additional parameters, namely by the onset frequency ω and the (zero) eigenvalue λ. The above dynamical system of seven equations is supplemented with three integral conditions on the functions $\rho_s(z)$, $C(z)$, and $S(z)$. These are given by Eqs. (12) and by the normalization condition on ρ_s,

$$\int_{z_0}^{L+z_0} \rho_s(z)\,dz = N, \quad (15)$$

where N is the normalization parameter. The boundary conditions for all involved functions are taken to be periodic in the interval $z \in [z_0, z_0 + L]$. This boundary value problem (BVP) of seven equations and three integral conditions is then solved using the numerical continuation technique in AUTO [41] (see Appendix A for details).

B. Stability thresholds

Before proceeding, it is important to notice that the linear stability of the stationary distribution ρ_s crucially depends on the choice of the coupling function $f(z)$ [see Eq. (2)]. Thus, the solution of the BVP Eqs. (14) is invariant under the shift of the coordinate system $z \to z + \delta$, with arbitrary δ, only if the coupling function $f(z)$ is itself periodic with the period L. Indeed, the integrals $\int_{z_0}^{z_0+L} f(z)C(z)\,dz$ and $\int_{z_0}^{z_0+L} f(z)S(z)\,dz$ are shift invariant if $f(z)$ is L periodic. On the contrary, if the period of $f(z)$ differs from L, or if $f(z)$ is a nonperiodic function, then the stability threshold depends on the particular choice of origin of the z axis, i.e., it depends on z_0. Following [27] we use a linear, nonperiodic coupling function $f(z) = z$. We note that this choice is motivated by recent experimental works [see, e.g., Refs. [16,23]]. Indeed, using video microscopy, it is possible to monitor the trajectories of individual colloidal particles and, therefore, also their center of mass. The center-of-mass position is precisely the quantity one obtains when inserting the relation $f(z) = z$ into Eq. (2) for the coupling function $\bar{f}(t)$. For further calculations, the origin of the z axis is chosen in the maximum of the washboard potential $U(z)$, implying that $z_0 = 0$.

First, we fix $\tau = 1$ and compute the stability threshold in the plane of parameters (γ, U_0), where $\gamma = F_0 - K_0 = 0$, for three different values of the coupling strength $K_0 = 7, 10, 12$, as shown in Fig. 1(a). The stationary density, normalized with $N = 1$, i.e., $\int_0^\pi \rho_s(z)\,dz = N = 1$, is unstable in the
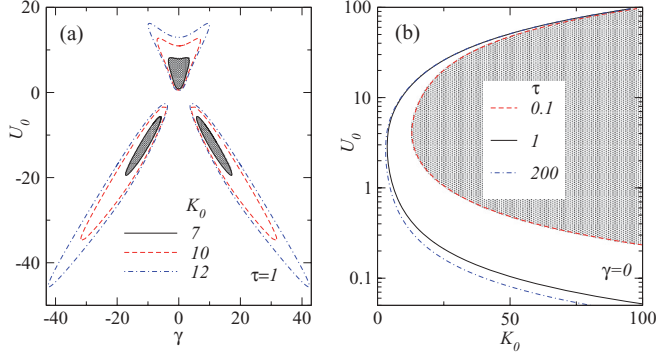
FIG. 1. (Color online) (a) Stability threshold in the plane (γ, U_0), obtained for $\tau = 1$ and different values of K_0, as given in the legend. The stationary state is unstable in the area enclosed by the respective curves (shaded area for $K_0 = 7$). (b) Stability threshold in the plane (K_0, U_0) for zero drive $\gamma = 0$ and different delay times as in the legend. The instability region always lies to the right from the respective curve (shaded area for $\tau = 0.1$).
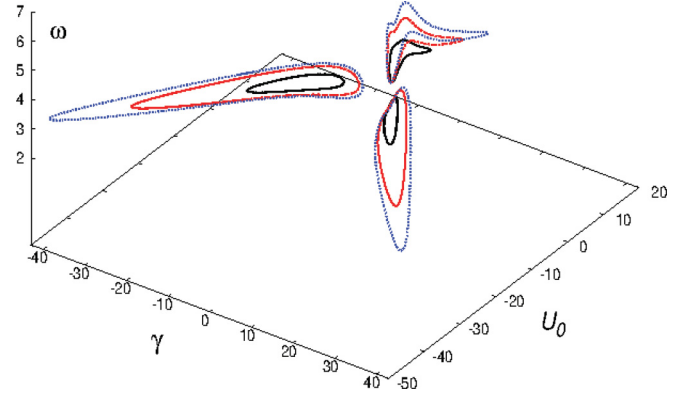

FIG. 2. (Color online) Three-dimensional view of Fig. 1(a). The onset frequency ω as a function of U_0 and γ for $\tau = 1$ and three different K_0. The projection onto the (γ, U_0) plane recovers Fig. 1(a).

C. Nonlinear regime: Numerical study of the one-body distribution

The observation of the linear instability with respect to oscillatory perturbations predicts possible deviations from the stationary state for a given ("overcritical") parameter set. In order to study the full nonlinear dynamics, however, the full Fokker-Planck equation of the system has to be solved. To explore these nonlinear effect we solve Eq. (4) numerically. Specifically, we employ a standard "forward-time centered-space" (FTCS) finite difference method [42] and integrate Eq. (4) starting from an inital distribution $\rho(z, t = 0)$.

As initial density distribution we choose the equilibrium density distribution in a one-dimensional washboard potential with periodic boundary conditions and the external bias, as well as the control, being switched off. This implies

$$\rho(z, t = 0) = \rho_0 \exp\left[-\beta U_0 \cos^2\left(\frac{z}{\sigma}\right)\right], \quad (16)$$

where ρ_0 ensures the normalization condition $\int_0^L \rho(z, t = 0)dz = N = 1$. We consider a fixed control amplitude, $K_0 = 7k_B T/\sigma$, and focus on parameter values near the stability threshold [see Fig. 1(a)]. Specifically, we consider the "balanced case" $\gamma = F_0 - K_0 = 0$ and washboard amplitude values of $U_0 = 8k_B T$ (linearly stable) and $U_0 = 7k_B T$ (linearly unstable), respectively. Beginning with the latter case, we plot in Fig. 3(a) snapshots of the density distribution $\rho(z, t)$ for three subsequent times. The initial distribution $\rho(z, t = 0)$ is periodic in the position coordinate z with a (spatial) period that is equal to the valley-to-valley distance of the washboard potential, that is, $\lambda_{wb} = \pi\sigma$. As expected, the values for the density distribution are increased at the position coordinates $z_i^{valley} = i\pi\sigma$ (where $i = [0,1,2,3,\ldots]$) corresponding to the valley positions of the washboard potential. The specific times t_1, t_2 are chosen such that the appertaining density distributions [shown as the dotted green curve and the dashed blue curve in Fig. 3(a), respectively] have a maximum displacement from the initial configuration. Inspecting the curves, we find that after a response time of roughly $5\tau_B$, the system settles indeed into a stable time-periodic density state, i.e., $\rho(z, t + T) = \rho(z, t)$, where the distribution oscillates around a washboard minimum position with a maximum displacement of approximately 0.33σ. The appearance of such stable

regions bounded by the corresponding closed curves. Thus, for $K_0 = 7$, the instability occurs in the shaded area. As expected, the area of the instability expands if the coupling strength K_0 is increased.

Interestingly, the stability diagram for the case when the origin of the z axis is chosen in the minimum of the washboard potential ($z_0 = \pi/2$) can be obtained from Fig. 1(a) by the transformation $U_0 \rightarrow -U_0$. For any other choice of z_0, the topology of the stability threshold is much more complex and generally contains four different bounded regions (not shown).

The effect of the time delay is demonstrated in Fig. 1(b) for the choice $\gamma = 0$. The stationary density is unstable in the area, which always stretches towards larger values of the coupling strength K_0, as shown by the shaded area for $\tau = 0.1$. Decreasing τ leads to the suppression of the instability, which clearly demonstrates that the instability is induced by the presence of the time delay in the coupling term.

However, it should be emphasized that having only a time-delayed coupling does not sufce to induce the instability. Thus, from Fig. 1(b) it follows that even if τ and K_0 are rather large, e.g., $\tau = 200$ and $K_0 \approx 100$, the stationary density is linearly stable for a vanishingly weak or an infinitely strong washboard potential U_0. At fixed K_0, only a certain combination of τ and U_0 renders the system unstable with respect to an oscillatory perturbation. Consequently, the onset of the synchronized time-periodic state is the effect of the combined action of the time-delayed coupling and stationary periodic external modulation in the form of the washboard potential.

By following the stability threshold in the parameter space, we additionally obtain the onset frequency ω directly on the threshold. The latter carries an important information about the time scale of the newly born oscillatory states, given by $T = 2\pi/\omega$. The three-dimensional view of Fig. 1(a), extended by the onset frequency ω, is shown in Fig. 2. It can be seen that the smallest temporal period $T \sim 1$ corresponds to positive U_0, whereas the period of the time-periodic states born at negative U_0 is up to threefold larger, i.e., $T \sim 6$.
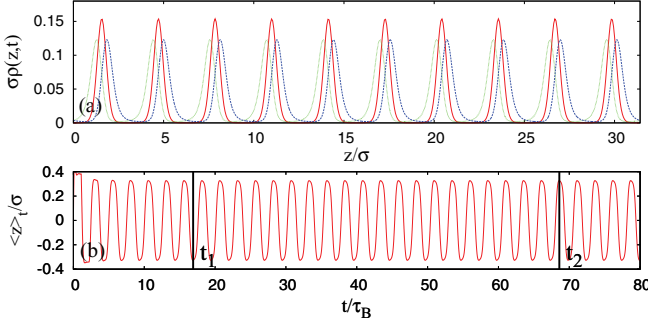
FIG. 3. (Color online) Results for a controlled system in the periodic regime. (a) Density distribution $\rho(z,t)$ as a function of position for selected times $t_0/\tau_B = 0$ (red curve), $t_1/\tau_B = 16.9$ (dotted green curve), and $t_2/\tau_B = 68.6$ (dashed blue curve). (b) Average particle position $\langle z \rangle_t$ as a function of time. The parameters are $U_0 = 7 k_B T$, $F_0 = 7 k_B T/\sigma$, $K_0 = 7 k_B T/\sigma$, $\tau = \tau_B$, and $L = 10\pi\sigma$.

oscillations is consistent with the stability diagram in Fig. 1(a). We supplement the discussion by plotting in Fig. 3(b) the particle position averaged over one period of the potential, that is, $\langle z \rangle_t = \int_0^{\lambda_{wb}} \rho(z,t)dz$. Clearly, $\langle z \rangle_t$ oscillates as a function of time with the same frequency ω as the frequency of the density oscillations. From now on, we therefore use the function $\langle z \rangle_t$ to obtain the cycle time $T = 2\pi/\omega$.

We now turn to the case $U_0 = 8 k_B T$. For this parameter, the perturbating forces, specifically the constant tilting force $\mathbf{F}^{\mathrm{bias}}$ and the feedback force $\mathbf{F}^{\mathrm{f.b.}}$, do not lead to an oscillating state. This is illustrated in Fig. 4. It is seen that the oscillations at early times are being damped, resulting in a stationary, nonperiodic density for times $t \gtrsim 400\tau_B$. In Fig. 4(a) we show the results for the stationary density profile as a dashed blue curve, as well as for two additional profiles, where the red and dotted green curves represent the initial and one intermediate state, respectively. As can be seen from Fig. 4(b), the average particle position $\langle z \rangle_t$, converges to a constant value $\langle z \rangle_{\mathrm{stat}}/\sigma \approx 0$. In other words, the density displacement related to the equilibrium position at each potential valley vanishes and, thus, the profiles for times $t_2/\tau_B = 400$ and $t_0/\tau_B = 0$ coincide.
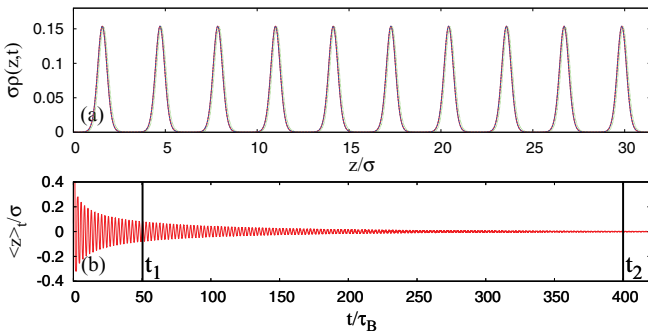

FIG. 4. (Color online) Results for a controlled system in the regime where the final state is stationary. (a) Density distribution $\rho(z,t)$ as a function of position for selected times $t_0/\tau_B = 0$ (red curve), $t_1/\tau_B = 50.4$ (dotted green curve), and $t_2/\tau_B = 400.0$ (dashed blue curve). (b) Average particle position $\langle z \rangle_t$ as a function of time. The parameters are $U_0 = 8 k_B T$, $F_0 = 7 k_B T/\sigma$, $K_0 = 7 k_B T/\sigma$, $\tau = \tau_B$, and $L = 10\pi\sigma$.
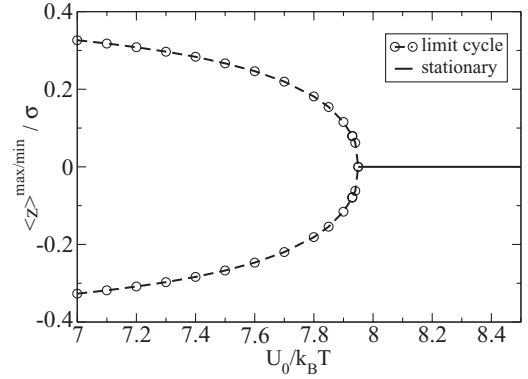

FIG. 5. Local extrema values of the function $\langle z \rangle_t$ as a function of the washboard amplitude U_0. The parameters are $F_0 = 7 k_B T/\sigma$, $K_0 = 7 k_B T/\sigma$, $\tau = \tau_B$, $L = 10\pi\sigma$.

We note that for both values of U_0 considered (cf. Figs. 3 and 4), the dynamics at early times is transient. In the oscillatory case, the transient regime lasts for about $t_{\mathrm{res}} \approx 5\tau_B$. For the linear stable case, the transient response time can be much larger. For example, for the parameter values that we considered in Fig. 4 the stationary state is not reached for times less than $t_{\mathrm{res}} \approx 400\tau_B$.

We have repeated the numerical calculations described above for a range of parameters U_0 and the choice $\gamma = F_0 - K_0 = 0$. In this way we can construct a bifurcation diagram characterizing the nature of the instability. As a measure of the instability, we use the oscillation amplitude of $\langle z \rangle_t$. Specifically, we obtain local extrema values $\langle z \rangle^{\mathrm{max}}$ and $\langle z \rangle^{\mathrm{min}}$ from the function $\langle z \rangle_t$ and average these over several periods. The results are summarized in Fig. 5. At large values of U_0, we only find one stable attracting fixed point $\langle z \rangle^{\mathrm{max}}$ and $\langle z \rangle^{\mathrm{min}} = 0$. However, by decreasing the washboard amplitude U_0 the stationary state (characterized by $\langle z \rangle^{\mathrm{max}}$ and $\langle z \rangle^{\mathrm{min}} = 0$ for all times t greater than the transient time) loses stability and stable limit cycle oscillations occur (see, e.g., Fig. 3). This happens in an essentially continuous manner, as Fig. 5 reveals. We thus conclude that, on decreasing U_0 below $U_0^c \approx 7.95 k_B T$, the system undergoes a supercritical Hopf bifurcation. For $U_0 < U_0^c$, all resulting trajectories perform limit cycle oscillations about the former stationary state $\langle z \rangle^{\mathrm{max}}$ and $\langle z \rangle^{\mathrm{min}} = 0$. We note that all neighboring trajectories approach the limit cycle. Thus, for $U_0 < U_0^c$, the limit cycle is stable and the only attractor in the system. Furthermore, due to the spatially left-right symmetry in the potential, the local extrema of $\langle z \rangle_t$ appear in symmetrical pairs at $\pm|\langle z \rangle^{\mathrm{max}}|$.

D. Cycle time for the oscillating density state

An interesting question is to which extent the density oscillation frequency depends on the different system parameters such as washboard potential amplitude U_0 and time delay τ. In Fig. 2 we have already shown results for the *onset* frequency based on the linear stability analysis. Here we present corresponding data obtained in the nonlinear regime. To this end we define the cycle time T as the overall travel time for a full maximum displacement of the density distribution (towards and back). As argued before, this time can be obtained
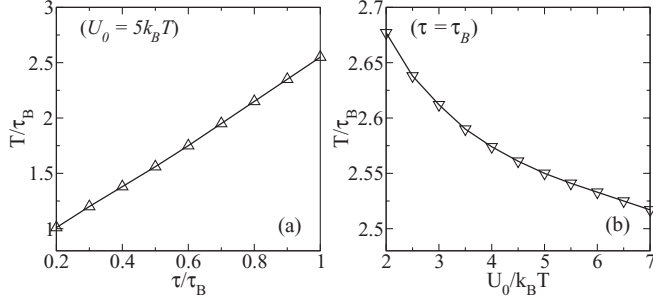
FIG. 6. Density oscillation cycle time T (a) as a function of the delay time τ and (b) as a function of the washboard potential amplitude U_0 within the oscillatory regime (see Fig. 1). The parameters are $F_0 = 7k_BT/\sigma$, $K_0 = 7k_BT/\sigma$, and $L = 10\pi\sigma$. The rest of the parameters as in the legend.

from the average particle position $\langle z \rangle_t$ by measuring the (time) distance between two maxima [see Fig. 3(b) for an example].

In Fig. 6(a) we plot the cycle time T as a function of the delay time τ. Clearly, by increasing the delay time τ the cycle time T increases as well. To understand this behavior, it is crucial to recall that the time-delayed feedback force incorporated here is of Pyragas type, i.e., a control target at time t and its value at time $t - \tau$ is used for the feedback signal. In our case, the control target is the center-of-mass position $\langle z \rangle_t$, which is being shifted as a function of time due to the constant force F^{bias}. Thus, a larger delay time τ implies that the system travels longer distances within the time interval τ. On the other hand, the specific form of the feedback force F^{fb} is constructed such that it always counteracts F^{bias} (see Eq. (1) and Refs. [27,31]). Furthermore, the absolute value of F^{fb} is small for large differences $\bar{f}(t) - \bar{f}(t - \tau)$. As a result, the crossover region where the feedback force F^{fb} changes from being essentially inactive to compensating the constant tilting force F^{bias} is accessed more often when the delay time is smaller. Thus, smaller delay times τ yield decreased cycle times T up to the limit where τ is too small to induce time-periodic oscillations in the density any longer [see Fig. 1(b)].

Figure 6(b) shows the dependence of T on the washboard amplitude U_0. It is seen that the cycle time T decreases slightly as a function of the washboard amplitude U_0. It is well known that the energy barrier plays a decisive role for the particle escape rate in a potential minimum for hopping processes that are thermally activated [43]. In our case, the interplay among the washboard potential, the constant tilting force, and the control force determines the rate at which particle are crossing to the next potential minimum. By increasing the washboard amplitude U_0, the energy barrier for a particle escape is increased, leading to smaller displacements of the average particle position in a valley. As a result, the cycle time of the oscillations is decreased.

IV. MICROCHANNEL GEOMETRY

So far we have considered infinite systems (i.e., systems with periodic boundaries). In this section we explore to which extent the emergence of an oscillation instability also depends on the channel geometry. To this end, we now consider a system that consists of a microchannel of finite length L with
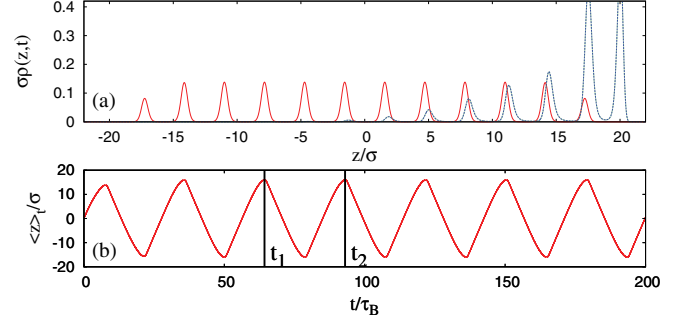

FIG. 7. (Color online) Results for the microchannel; (a) density distribution $\rho(z,t)$ as a function of position for selected times $t_0/\tau_B = 0$ (red curve), $t_1/\tau_B = 64.3$ (dotted green curve), and $t_2/\tau_B = 93.0$ (dashed blue curve), and (b) shows the first moment of $\rho(z,t)$ as a function of time. The parameters are $U_0 = 8k_BT$, $F_0 = 7k_BT/\sigma$, $K_0 = 7k_BT/\sigma$, $\tau = \tau_B$, and $z_{\text{wall}} = \pm 20\sigma$.

hard walls at the ends. A similar finite system (yet with particle interactions) has also been considered in our earlier study on a feedback-controlled colloidal system [27]. Here we instead focus on the nature of the oscillations and the corresponding instability as opposed to the corresponding phenomenon in the system with periodic boundaries. We choose as initial distribution the equilibrium density distribution for a single particle subject to the washboard potential plus a wall potential, $\beta U^{\text{wall}} = 10(z/z_{\text{wall}})^{20}$, which confines the particle position to values $|z| \lesssim z_{\text{wall}} = 20\sigma$. Such a smooth wall potential is typically used to model situations where the diameter of the particles forming the wall is much smaller than that of the fluid particles [44]. Thus, the initial distribution is given by

$$\rho(z,t=0) = \rho_0 \exp\left[-\beta U_0 \cos^2\left(\frac{z}{\sigma}\right) - 10\left(\frac{z}{z_{\text{wall}}}\right)^{20}\right].$$
(17)

Again, we focus on the "balanced case" $\gamma = F_0 - K_0 = 0$ with a fixed control amplitude value of $K_0 = 7k_BT/\sigma$. We recall that in the case of the infinite system (periodic boundaries) a washboard amplitude value of $U_0 = 8k_BT$ is already sufficient to suppress oscillatory states, yielding a stationary state for times larger than the transient response time. We choose this specific value for U_0 as a starting point for the microchannel study. In Fig. 7(a) we show snapshots of the density distribution at three different times, $t_0 = 0\tau_B$, $t_1 = 64.3\tau_B$, and $t_2 = 93.0\tau_B$. We note that the initial density distribution $\rho(z,t=0)$ (shown as a red curve) is symmetric with respect to the position $z = 0$. After a transient response time of roughly $20\tau_B$ we find stable time-periodic density oscillations where the distribution oscillates between two states characterized by a low and a high average particle position, respectively. Therefore, this state fulfills the periodicity condition $\rho(z,t+T) = \rho(z,t)$ with $T = 2\pi/\omega$ being the cycle time of the oscillations. The snapshots at times t_1 and $t_2 = t_1 + T$ [shown as a dotted green and a dashed blue curve in Fig. 7(a), respectively] reveal that, indeed, both density profiles appear to be identical, at least to the naked eye. We support this conclusion by plotting in Fig. 7(b) the average particle position $\langle z \rangle_t = \int_0^L z\rho(z,t)dz$ as a function
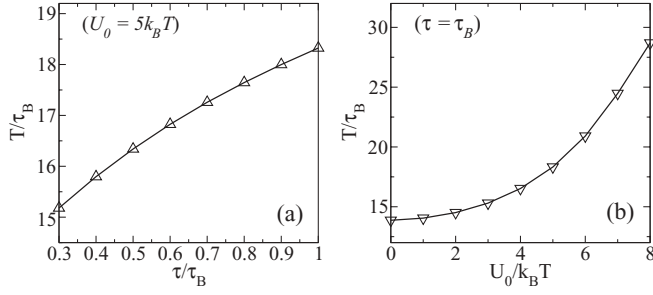
FIG. 8. Density oscillation cycle time T for the microchannel as (a) function of the delay time τ and (b) function of the washboard potential amplitude U_0. The parameters are $F_0 = 7k_BT/\sigma$, $K_0 = 7k_BT/\sigma$, and $z_{\mathrm{wall}} = \pm20\sigma$. The rest of the parameters as in the legend.

of time. Here, the function $\langle z \rangle_t$ is averaged over the entire channel length L in contrast to the circular ring geometry (periodic boundaries) where the obtained results are periodic with respect to each valley position. Similarly as in Sec. III C, the function $\langle z \rangle_t$ oscillates as a function of time with the same frequency ω as the frequency of the density oscillations, as can be seen from the time stamps t_1 and $t_2 = t_1 + T$, which we have included as vertical lines. However, we stress that the cycle times here are much longer than for the circular ring geometry. Furthermore, the periodic states have the spatial period equal to the largest spatial period used in the system, which is the system length itself as imposed by the wall potential. As a result, the time-periodic solution oscillates back and forth between $z = \pm z_{\mathrm{wall}}$. We also note that the finding of density oscillations for $U_0 = 8k_BT$, $\gamma = 0$, and $\tau = \tau_B$ is in contrast to what we found in Sec. III C where no (periodic) instabilities occur for this specific parameter set.

By further increasing the washboard amplitude to the value of $U_0 = 9k_BT$, on the other hand, we find that the oscillatory behavior at early times is being damped, resulting in a stationary, nonperiodic density for times $t \gtrsim 20\tau_B$. We conclude that the results of the linear stabilty analysis (cf. Fig. 1) can approximately be used as a reference to find states that are linearly unstable for the microchannel system. We argue that this is because the channel is so large ($L = 44\sigma$) that the system is mostly determined by the bulk properties. The instability region for the finite channel seems to be qualitatively similar but increased in size compared to the results for the circular ring geometry.

In Fig. 8(a) we show results for the cycle time T as a function of the delay time τ for a fixed value of $K_0 = 7k_BT/\sigma$ and the choice $\gamma = F_0 - K_0 = 0$. Holding the washboard potential amplitude fixed to the value of $U_0 = 5k_BT$, we do not find oscillatory density states below $\tau = 0.3\tau_B$. By increasing τ, we find a qualitatively similar behavior as in the periodic system (see Sec. III D) for the cycle time T. Specifically, we find a monotonic increase on T as a function of τ. On the other hand, quantitatively comparing the results for the cycle time T to the periodic system reveals that the values increase by approximately one order of magnitude. This is clearly a consequence of the substantial differences in the oscillations that we observe for the microchannel: The underlying nonlinear terms in the dynamical equations [see
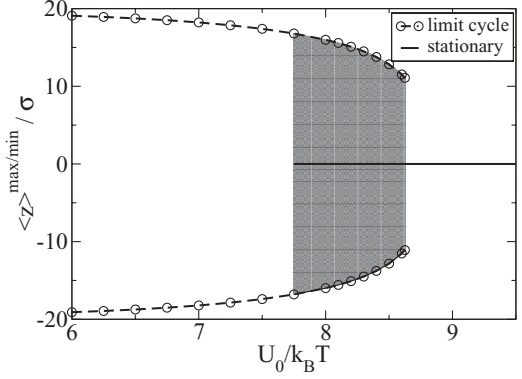

FIG. 9. Local extrema values of the function $\langle z \rangle_t$ as a function of the washboard amplitude U_0. The shaded area marks the region where the system exhibits hysteresis. The parameters are $F_0 = 7k_BT/\sigma$, $K_0 = 7k_BT/\sigma$, $\tau = \tau_B$, $z_{\mathrm{wall}} = \pm20\sigma$.

Eqs. (3) and (4)] drive the density propagations over the whole system size, which is given by the channel length L. Thus, it is clear that the cycle time must be significantly longer than in the periodic system, where the oscillations occur around a valley position with displacements that are smaller than $\pi\sigma$ (the spatial period of the washboard potential). We note that for the τ values that we considered (up to $\tau = 10\tau_B$), we do not find any upper boundary for the linear stability threshold. This behavior seems to be similar to the periodic system, where we showed that the oscillatory density state cannot be transformed into a stationary state by increasing the value of τ [cf. Fig. 1(b)].

In order to investigate the dependence of the cycle time T on the washboard amplitude U_0, we hold the delay time fixed to the value of $\tau = \tau_B$ and increase (decrease) U_0 in steps of $\Delta U_0 = 1k_BT$ towards the linear stability threshold. We do not find oscillatory density states above $U_0^c \approx 8.63k_BT$. Furthermore, we observe a monotonic *increase* of T as a function of U_0, which contrasts with the periodic system where we found monotonic decrease. Again, this is a consequence of the substantially different oscillation mode that we observe for the microchannel.

As explained above, any oscillatory perturbation applied to the system travels over the whole system length. Thus, an increased value of U_0 now means that the propagation of the perturbation is hindered, which results in an increased cycle time T that corresponds to the travel time over a distance of approximately twice the system length L (see Sec. III D).

For completeness, we show in Fig. 9 the bifurcation diagram for the microchannel calculated in the same fashion as in Sec. III C. We find only stationary states for washboard amplitudes $U_0 > U_0^c$. Contrary to the infinite system, however, the average particle position $\langle z \rangle_t$ in this stationary state is principally a *nonzero* constant as $t \to \infty$. For simplicity, all stationary states in Fig. 9 have been shifted to zero. On increase of U_0 all density oscillations suddenly drop off at $U_0 = U_0^c$ with a jump in the (oscillation) amplitude from the value $|\langle z \rangle^{\mathrm{max}}|$ to zero; i.e., a *subcritical* Hopf bifurcation occurs. As the parameter U_0 is reversed, a stationary solution can be found below the Hopf bifurcation point for values ranging to $U_0^m \approx 7.75k_BT$. Thus, the system system exhibits hysteresis

within the parameter region $U_0^m < U_0 < U_0^c$ (shown as the shaded area in Fig. 9).

V. INFLUENCE OF REPULSIVE PARTICLE INTERACTIONS

In many real colloidal systems, interactions between the particles cannot be neglected. In this last paragraph, we briefly consider the case of purely repulsive interactions. Contrary to Ref. [27], which involved finite systems, we here consider a system with periodic boundaries (see Sec. III for the corresponding noninteracting case). To this end, we utilize the recently developed DDFT. The DDFT key equation is given by [45–47]

$$\Gamma^{-1} \frac{\partial \rho(z,t)}{\partial t} = \nabla \left[\rho(z,t) \nabla \frac{\delta \mathcal{F}[\rho(z,t)]}{\delta \rho(z,t)} \right]. \quad (18)$$

The mobility coefficient in Eq. (18) is the same as in the Fokker-Planck approach [see Eq. (4)], i.e., we can set its value to $\Gamma \tau_B k_B T / \sigma^2 = 1$. The chemical potential $\mu(z,t)$ obtained from the Helmholtz free energy functional $\mathcal{F}$ has three contributions,

$$\mu(z,t) = \frac{\delta \mathcal{F}[\rho(z,t)]}{\delta \rho(z,t)} = \mu_{\text{id}}(z,t) + \mu_{\text{int}}(z,t) + \mu_{\text{ext}}(z,t). \quad (19)$$

The first contribution is the ideal gas term $\mu_{\text{id}} = k_B T \ln \Lambda \rho(z,t)$ (Λ denotes the thermal de Broglie wavelength), the second contribution μ_{int} accounts for particle interactions, and the third contribution is the external potential $\mu_{\text{ext}} = U_{\text{ext}}$, which in our case includes the contributions from the tilted washboard potential and the control force [see Eq. (3)]. In the following, the colloidal interactions are treated within a mean-field approach, that is, $\mu_{\text{int}}(z) = \int dz' \rho(z',t) U^{\text{rep}}(|z - z'|)$. We employ the Gaussian core model (GCM), where the interaction potential is given by $U^{\text{rep}}(|z - z'|) = \varepsilon_0 \exp[-(z - z')^2/\sigma^2]$. The GCM represents a typical coarse-grained potential which describes a wide class of *soft* macroparticles with effective (gyration) radius σ [48,49]. We choose positive repulsion strengths $\varepsilon_0 > 0$, such that the interaction is purely repulsive. Also, we focus in this section on the circular ring geometry (periodic boundaries) and consider the case of $N = 2$.

We note that, even in the noninteracting case, the results from the linear stability analysis (see Sec. III A) cannot be used as a basis for comparison. The reason is that the calculations in Sec. III A were done with $N = 1$. Rather, the washboard amplitude U_0 must be increased significantly to find a stable stationary state. For example, for the "balanced case," $\gamma = F_0 - K_0 = 0$ (and $\varepsilon_0 = 0$), we find oscillatory density states for a broad spectrum of values for U_0 ranging up to $U_0 \approx 14 k_B T$ (recall that $U_0 = 8 k_B T$ is sufficient to suppress oscillatory states for $N = 1$ and the rest of the parameters being the same).

In Fig. 10 we show results for the average particle position $\langle z \rangle_t$ for $U_0 = 15 k_B T$ (and $N = 2$). In the case of the noninteracting system $\varepsilon_0 = 0$ (shown as a solid curve in Fig. 10) the function $\langle z \rangle_t$ is indeed being damped as a function of time, reflecting a stationary state for times larger than the transient response time, which is here of the order of $t_{\text{res}} \approx 2000 \tau_B$.
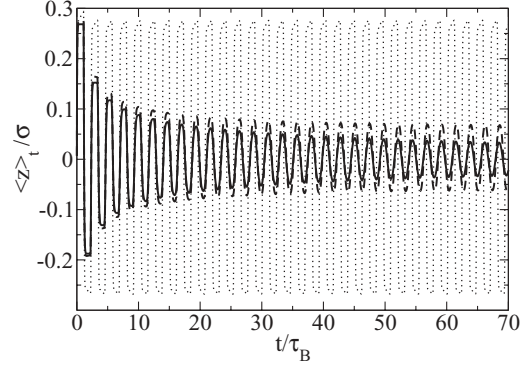

FIG. 10. Results for the average particle position $\langle z \rangle_t$ as a function of time for different repulsion strengths: $\varepsilon_0 = 0 k_B T$ (solid curve), $\varepsilon_0 = 12 k_B T$ (dashed curve), and $\varepsilon_0 = 15 k_B T$ (dotted curve). The parameters are $U_0 = 15 k_B T$, $F_0 = 7 k_B T / \sigma$, $K_0 = 7 k_B T / \sigma$, $\tau = \tau_B$, $L = 10\pi\sigma$, and $N = 2$.

On increase of the repulsion strength ε_0, the extrema of the function $\langle z \rangle_t$ increase (see the dashed curve and the dotted curve in Fig. 10, respectively). This is consistent with our earlier finding [27] that repulsive interactions support the particles in crossing the barrier, yielding an increase of the long-time diffusion coefficient. Moreover, for $\varepsilon_0 = 15 k_B T$, we find stable (time-periodic) density oscillations with cycle time $T = 2.315 \tau_B$. Thus, repulsive interparticle interactions can be successfully used to stabilize the oscillatory density state. We note, however, that for the present system, increasing the average density (via the particle number N) has a considerably greater impact on the linear stability of the system.

VI. CONCLUDING REMARKS

In the present work, we have investigated the dynamics of colloidal particles subject to a one-dimensional, tilted washboard potential under time-delayed feedback control. The major goal was to identify conditions under which the control can induce oscillatory states. The latter are absent in the uncontrolled system. Our investigations are based on the (nonlinear) Fokker-Planck equation, combined with a linear stability analysis.

We have investigated infinite systems (i.e., systems with periodic boundaries) and microchannels of finite length L (bounded by repulsive walls). For the first case, we have obtained, based on linear stability analysis, a full state diagram. This diagram predicts that oscillations (of the density field) do indeed occur for finite values of the delay time and control strengths comparable to the strengths of the conservative forces. Investigating the time dependence of the same system via numerical solution of the Fokker-Planck equation, we found full consistency with the results of the linear stability analysis for all model parameters considered. In addition, the numerical solution provides results for the (likewise oscillating) moments of the density distribution. In particular, from the oscillations of the first moment (i.e., the current) we could identify the cycle time. The latter was found to monotonically decrease with the delay time.

In the finite system (which we have investigated via the full Fokker-Planck equation alone), we also found

oscillations. However, the spatial extension of these oscillations corresponds to the wall-to-wall separation rather than to the width of one valley, as in the infinite-system case. Despite these differences, the parameter region where the finite system exhibits feedback-induced oscillations is rather similar to that found in the infinite case. We attribute this to the fact that the finite system under consideration was still so large ($L \gg \lambda_{wb} = \pi\sigma$) that boundary effects are not dominant. Finally, we have briefly considered the case that the colloidal particles interact. This was done on the basis of the recently developed DDFT [45–47], a generalized continuity equation where the particle interactions enter via a free energy functional. Using a purely repulsive (GCM) pair potential, we have shown that such interactions can *stabilize* oscillatory states. However, to see this effect, the strength of repulsion must be of the order of the washboard amplitude (and both must be significantly larger than $k_B T$). Taken together, we have shown that colloidal particles in modulated potentials under time-delayed feedback control can display highly nontrivial dynamics, particularly oscillations. One way to understand these differences to the uncontrolled case is that our feedback control term, which relies on the average particle position and, thus, involves *all* particles, introduces effectively time-dependent interactions between the particles.

We note that feedback-induced spatiotemporal effects have been recently also been found in other extended systems such as optical resonators, where the delayed feedback generates spontaneous motion of cavity solutions [32] and, more generally, systems describable by the Swift-Hohenberg equation [50]. A particularly interesting feature of the present colloidal system is that it is, in principle, accessible by experiments [16–18]. Indeed, colloidal particles are typically so large that their position (and, consequently, the first moment of the density distribution) can be easily monitored by real-space methods such as video microscopy. We therefore hope that our results will stimulate future experiments. Moreover, from the theoretical side one could extend the present analysis to mixtures consisting of several species with multiple time delay constants. This could be a promising route for the development of a novel particle sorting effect in narrow channels.

APPENDIX: NUMERICAL CONTINUATION OF SOLUTIONS OF THE LINEARIZED FOKKER-PLANCK EQUATION

It is known that in order to continue any given solution of the boundary value problem (BVP) mentioned in Sec. III A with 7 equations, 7 boundary conditions, and 3 integral conditions, one requires $(7 + 3 - 7 + 1 = 4)$ continuation parameters. We always include the pair (ω, λ) into the set of continuation parameters. Consequently, we are left only with two additional continuation parameters. These can be chosen in the arbitrary fashion out of the set (U_0, K_0, F_0, τ, N). For example, the solution of the BVP can be continued in the plane of (U_0, K_0), with all other parameters fixed. The result of such continuation is a line in the space (U_0, K_0). Generally, any continuation yields a co-dimension 1 manifold in the space of system parameters, which represents the stability threshold. The onset frequency ω is then an output parameter, which is given by a certain function of the position on the threshold. The accuracy of all continuation runs is controlled by checking that the absolute value of the eigenvalue λ is of the order of $10^{-10} \ldots 10^{-12}$.

Generally, it is not easy to find a particular combination of the system parameters directly on the stability threshold and, additionally, to correctly guess the corresponding value of ω. In order to find a starting point for our continuations, we employ the following strategy. First, we switch off the integral conditions Eqs. (12) and continue an analytically known solution at vanishing driving force ($F_0 = 0$), that is,

$$\rho_s(z) \sim e^{-U(z)}, \quad C(z) = 0, \quad S(z) = 0, \qquad \text{(A1)}$$

with an arbitrary guess of τ and ω in parameter ω, until the point $\langle S \rangle = 0$ is found. Second, we continue this solution in parameter K_0, until the point on the stability threshold is found, i.e., $\langle S \rangle = 0$ and $\langle C \rangle = 1$. Note that the condition $\langle S \rangle = 0$ remains unaffected, when continuing in the parameter K_0. Finally, we switch the integral conditions Eqs. (12) back on and proceed with the continuation in any of the parameters (U_0, K_0, F_0, τ, N), as described above.

[1] P. Hänggi and F. Marchesoni, Rev. Mod. Phys. **81**, 387 (2009).

[2] P. S. Burada, P. Hänggi, F. Marchesoni, G. Schmid, and P. Talkner, Chem. Phys. Chem. **10**, 45 (2009).

[3] S.-H. Lee and D. G. Grier, Phys. Rev. Lett. **96**, 190601 (2006).

[4] V. Blickle, T. Speck, U. Seifert, and C. Bechinger, Phys. Rev. E **75**, 060101 (2007).

[5] C. Dalle-Ferrier, M. Kruger, R. D. L. Hanes, S. Walta, M. C. Jenkins, and S. U. Egelhaaf, Soft Matter **7**, 2064 (2011).

[6] R. D. L. Hanes, C. Dalle-Ferrier, M. Schmiedeberg, M. C. Jenkins, and S. U. Egelhaaf, Soft Matter **8**, 2714 (2012).

[7] A. Ros, R. Eichhorn, J. Regtmeier, T. T. Duong, P. Reimann, and D. Anselmetti, Nature **436**, 928 (2005).

[8] R. Gommers, V. Lebedev, M. Brown, and F. Renzoni, Phys. Rev. Lett. **100**, 040603 (2008).

[9] P. Tierno, P. Reimann, T. H. Johansen, and F. Sagués, Phys. Rev. Lett. **105**, 230602 (2010).

[10] P. Reimann, Phys. Rep. **361**, 57 (2002).

[11] P. Reimann, C. Van den Broeck, H. Linke, P. Hänggi, J. M. Rubi, and A. Pérez-Madrid, Phys. Rev. Lett. **87**, 010602 (2001).

[12] K. Lindenberg, J. M. Sancho, A. M. Lacasta, and I. M. Sokolov, Phys. Rev. Lett. **98**, 020602 (2007).

[13] J. Jordanovic, S. Jäger, and S. H. L. Klapp, Phys. Rev. Lett. **106**, 038301 (2011).

[14] A. Zaccone, H. Wu, and E. Del Gado, Phys. Rev. Lett. **103**, 208301 (2009).

[15] P. Chaudhuri, L. Berthier, and W. Kob, Phys. Rev. Lett. **99**, 060604 (2007).

[16] M. Evstigneev, O. Zvyagolskaya, S. Bleil, R. Eichhorn, C. Bechinger, and P. Reimann, Phys. Rev. E **77**, 041107 (2008).

[17] F. J. Cao, L. Dinis, and J. M. R. Parrondo, Phys. Rev. Lett. **93**, 040603 (2004).

[18] A. V. Arzola, K. Volke-Sepúlveda, and J. L. Mateos, Phys. Rev. Lett. **106**, 168104 (2011).

[19] W. Mu, Z. Liu, L. Luan, G. Wang, G. C. Spalding, and J. B. Ketterson, New J. Phys. **11**, 103017 (2009).

[20] X. X. Sun, L. R. Nie, and P. Li, Europhys. Lett. **95**, 50003 (2011).

[21] L.-C. Du and D.-C. Mei, J. Stat. Mech.: Theory Exp. (2011) P11016.

[22] E. M. Craig, B. R. Long, J. M. R. Parrondo, and H. Linke, Europhys. Lett. **81**, 10002 (2008).

[23] B. J. Lopez, N. J. Kuwada, E. M. Craig, B. R. Long, and H. Linke, Phys. Rev. Lett. **101**, 220601 (2008).

[24] T. Sagawa and M. Ueda, Phys. Rev. E **85**, 021104 (2012).

[25] D. Abreu and U. Seifert, Phys. Rev. Lett. **108**, 030601 (2012).

[26] S. Toyabe, T. Sagawa, M. Ueda, E. Muneyuki, and M. Sano, Nature Physics **6**, 988 (2010).

[27] K. Lichtner and S. H. L. Klapp, Europhys. Lett. **92**, 40007 (2010).

[28] E. Schöll and H. Schuster, *Handbook of Chaos Control* (John Wiley & Sons, New York, 2007).

[29] K. Pyragas, Phys. Lett. A **170**, 421 (1992).

[30] D. Hennig, L. Schimansky-Geier, and P. Hänggi, Phys. Rev. E **79**, 041117 (2009).

[31] D. Hennig, Phys. Rev. E **79**, 041114 (2009).

[32] M. Tlidi, A. G. Vladimirov, D. Pieroux, and D. Turaev, Phys. Rev. Lett. **103**, 103904 (2009).

[33] P. T. Korda, M. B. Taylor, and D. G. Grier, Phys. Rev. Lett. **89**, 128301 (2002).

[34] K. Xiao and D. G. Grier, Phys. Rev. E **82**, 051407 (2010).

[35] L. Lizana and T. Ambjörnsson, Phys. Rev. E **80**, 051103 (2009).

[36] H. Löwen, J. Phys.: Condens. Matter **21**, 474203 (2009).

[37] A. Pototsky, A. J. Archer, S. E. Savel'ev, U. Thiele, and F. Marchesoni, Phys. Rev. E **83**, 061401 (2011).

[38] H. Risken, *The Fokker-Planck Equation: Methods of Solutions and Applications*, Springer Series in Synergetics, 2nd ed. (Springer, Berlin, 1996).

[39] A. Pototsky and N. Janson, Physica D **238**, 175 (2009).

[40] A. Pototsky, Phys. Rev. E **85**, 036219 (2012).

[41] E. Doedel, R. Paffenroth, A. R. Champneys, T. F. Fairgrieve, Y. A. Kuznetsov, B. Sandstede, and X. Wang, Technical Report, Caltech (2001).

[42] W. H. Press, S. A. Teukolsky, W. T. Vetterling, and B. P. Flannery, *Numerical Recipes: The Art of Scientific Computing*, 3rd ed. (Cambridge University Press, New York, 2007).

[43] H. Kramers, Physica **7**, 284 (1940).

[44] S. Grandner and S. H. L. Klapp, J. Chem. Phys. **129**, 244703 (2008).

[45] U. M. B. Marconi and P. Tarazona, J. Phys.: Condens. Matter **12**, A413 (2000).

[46] U. M. B. Marconi and P. Tarazona, J. Chem. Phys. **110**, 8032 (1999).

[47] A. J. Archer and R. Evans, J. Chem. Phys. **121**, 4246 (2004).

[48] C. Likos, Phys. Rep. **348**, 267 (2001).

[49] A. A. Louis, P. G. Bolhuis, and J. P. Hansen, Phys. Rev. E **62**, 7961 (2000).

[50] S. V. Gurevich and R. Friedrich, arXiv:1206.7059v3 (2012).